Electronic Supplementary Information (ESI)

Paradoxical role of structural degradation of nickel-rich layered oxides in capacity retention upon storage of lithium-ion batteries

Hyejeong Hyun[1§], Hyojung Yoon[2§], Subin Choi[1], Juri Kim[2], So Young Kim[2], Tom Regier[3], Zachary Arthur[3], SeokKoo Kim[2], Jongwoo Lim[1]*

[1] Department of Chemistry, Seoul National University, Seoul, 08826, Republic of Korea

[2] Battery Research Center, LG Energy Solution, Daejeon, 34122, Republic of Korea

[3] Canadian Light Source, University of Saskatchewan 44 Innovation Boulevard, Saskatoon, SK S7N 2V3, Canada

*Corresponding author: jwlim@snu.ac.kr

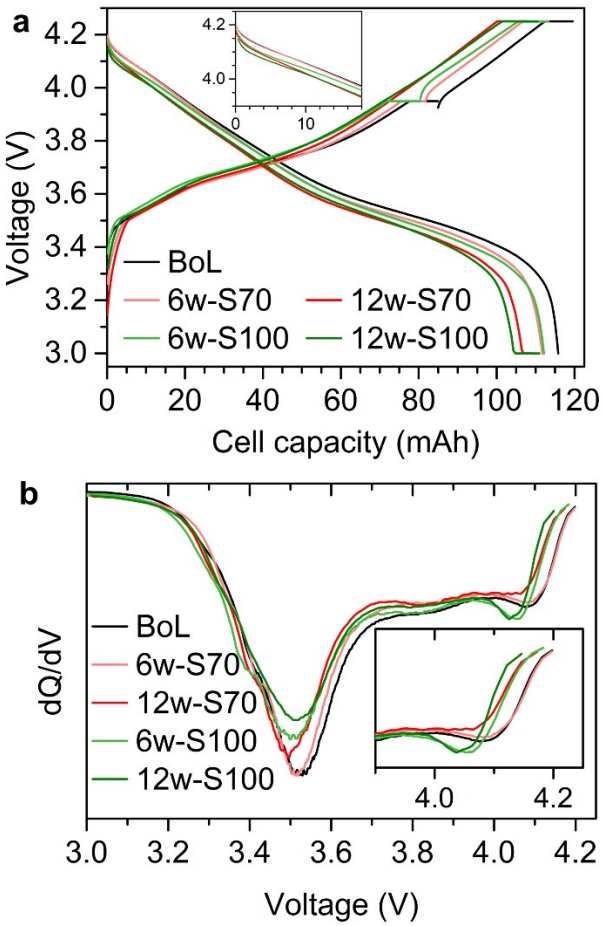

Fig. S1 a Voltage profiles of NCM6/graphite pouch cells during *operando* XRD experiments (Fig. 2 and Fig. 3). **b** dQ/dV profile during discharge. The pouch cells were CCCV charged (CCCV cutoff 0.05C) at C/3 and CC discharged at C/3 (1C = 120 mA), in the voltage range of 3.0–4.25 V.

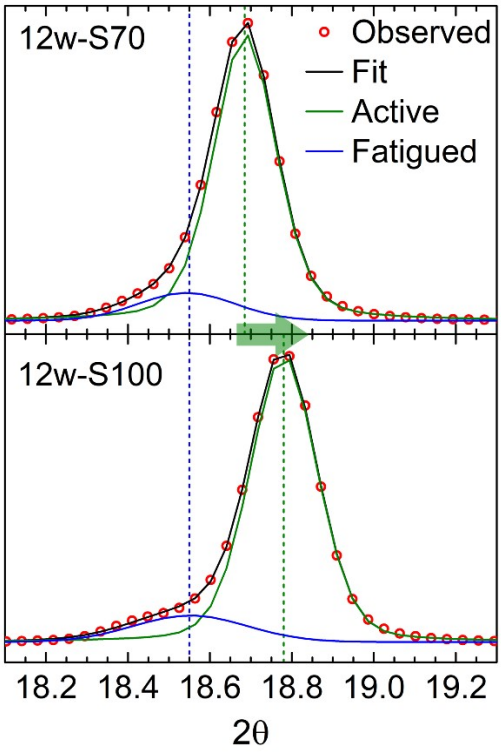

Fig. S2 Representative examples of deconvolution of *operando* XRD pattern of (003) Bragg peak of NCM6 cathodes at the charge endpoint of NCM6/graphite cells.

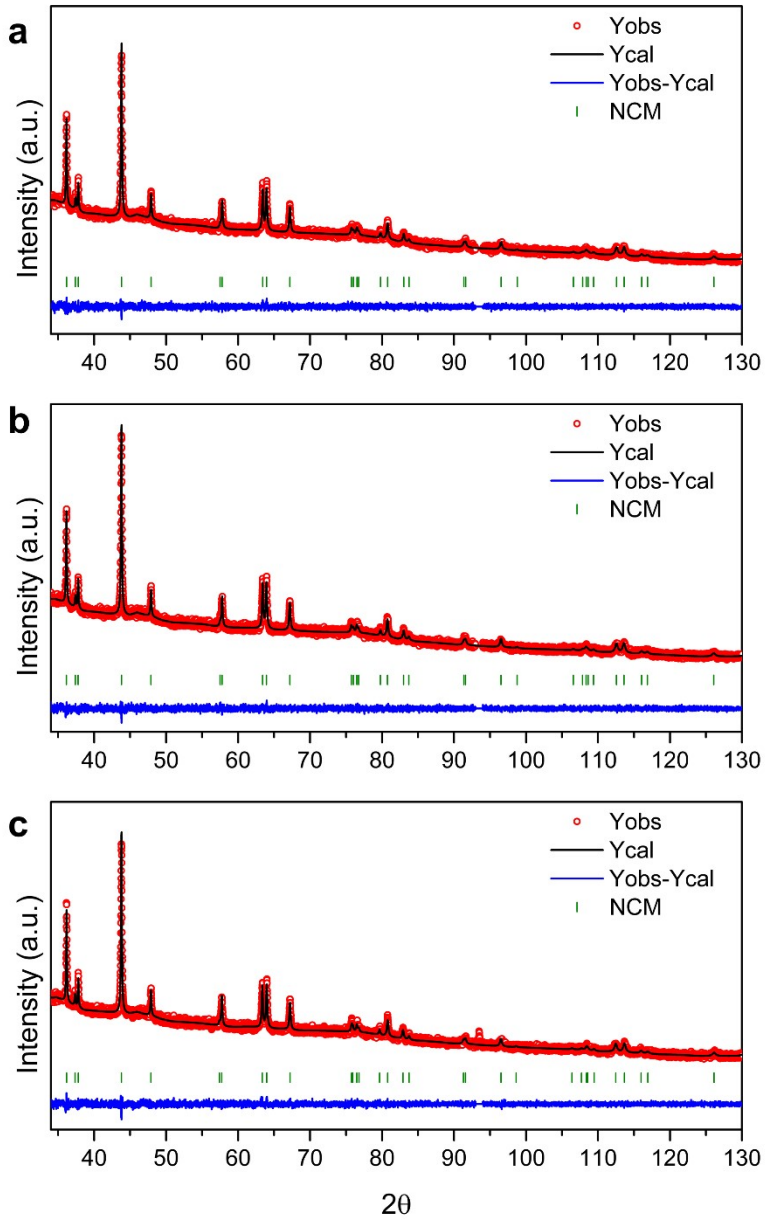

Fig. S3 Ex situ SXRD patterns of **a** BoL, **b** 12w-S70, and **c** 12w-S100 NCM6 cathodes at the discharge endpoint. The signals at a low 2θ region (< 35°) were excluded due to the strong background signal.

Table S1 Rietveld refinement results of ex situ SXRD patterns (Fig. S3) of NCM6 cathodes at the discharge endpoint. As the z-coordinate of O (z_O) in 6c sites only can be varied, other atomic coordinates of 3a and 3b sites are omitted hereafter.

	BoL	**12w-S70**	**12w-S100**
a (Å)	2.87174(6)	2.87201(5)	2.87064(5)
c (Å)	14.2296(3)	14.2300(3)	14.2484(3)
V ($Å^3$)	101.628(4)	101.650(3)	101.684(3)
z_O	0.2591(3)	0.2589(3)	0.2596(3)
TM_{Li}	0.027(2)	0.031(1)	0.023(2)
R_{Bragg}	2.42	2.49	3.06
χ^2	1.12	1.14	1.13

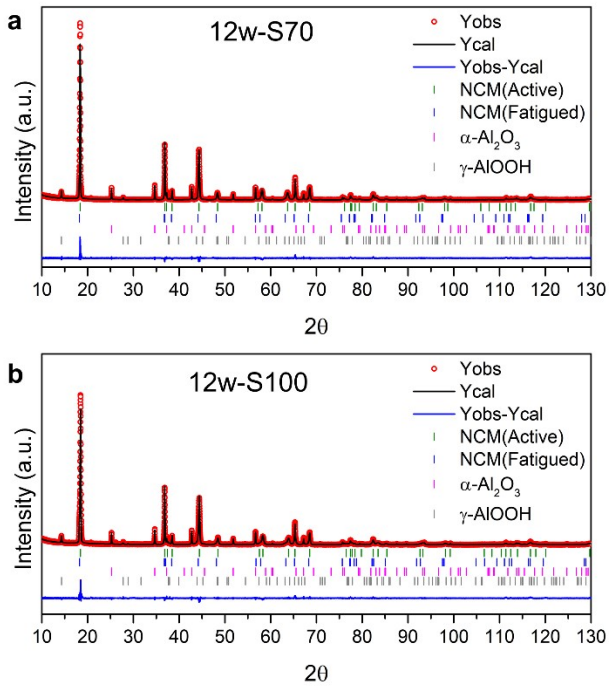

Fig. S4 Rietveld refinement of ex situ SXRD patterns of 12-week-stored NCM6 cathodes at the charge endpoint (CCCV charged to 4.3 V versus Li, with the voltage hold until current decays to 0.01C). **a** 12w-S70 and **b** 12w-S100. Two additional phases, α-Al_2O_3 and γ-AlOOH, were included for profile fitting, since the alumina-coated separator was used in the cells and coated ceramic was partially transferred onto the cathode surface.

Table S2 Rietveld refinement results of the 12w-S70, 12w-S100 NCM6 cathodes at the charge endpoint (Fig. S4). The phase fractions of active and fatigued phases were recalculated excluding those of α-Al_2O_3 and γ-AlOOH.

	BoL	12w-S70		12w-S100	
		Active	Fatigued	Active	Fatigued
a (Å)	2.81725(1)	2.81714(1)	2.8253(2)	2.81849(2)	2.82357(8)
c (Å)	14.3114(2)	14.2917(1)	14.4298(11)	14.2228(2)	14.3911(14)
V (Å^3)	98.370(2)	98.227(1)	99.753(11)	97.847(2)	99.362(10)
z_O	0.26745(8)	0.26671(8)	0.2779(13)	0.26677(9)	0.27213(48)
R_{Bragg}	8.53	5.54	3.89	5.97	3.10
Fraction(%)	100	94.8(5)	5.2(3)	84.7(6)	15.3(4)
χ^2	3.24	2.53		2.47	

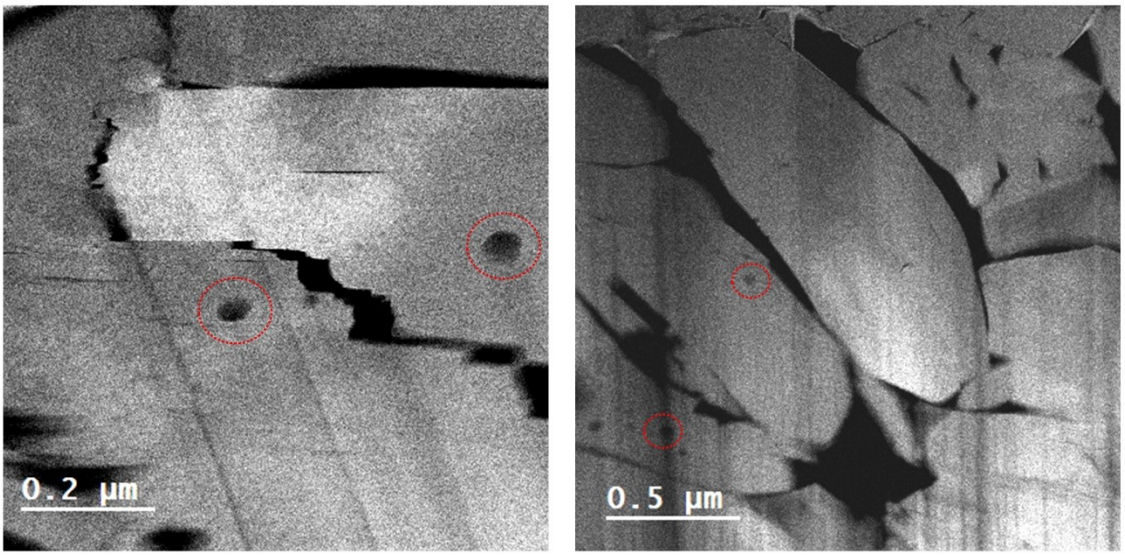

Fig. S5 TEM images of the 12w-S100 NCM6 cathode.

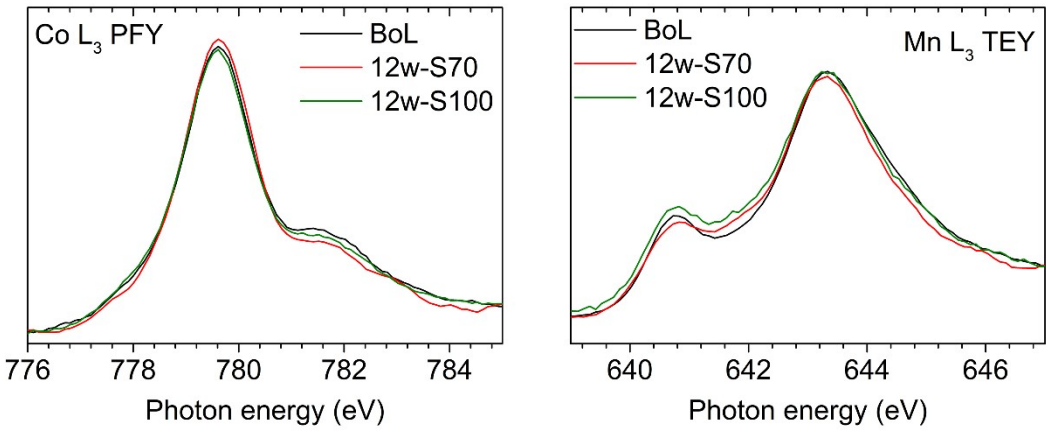

Fig. S6 Co L_3-edge PFY and Mn L_3-edge TEY spectra of the 12-week-stored NCM6 cathodes at the charge endpoint.

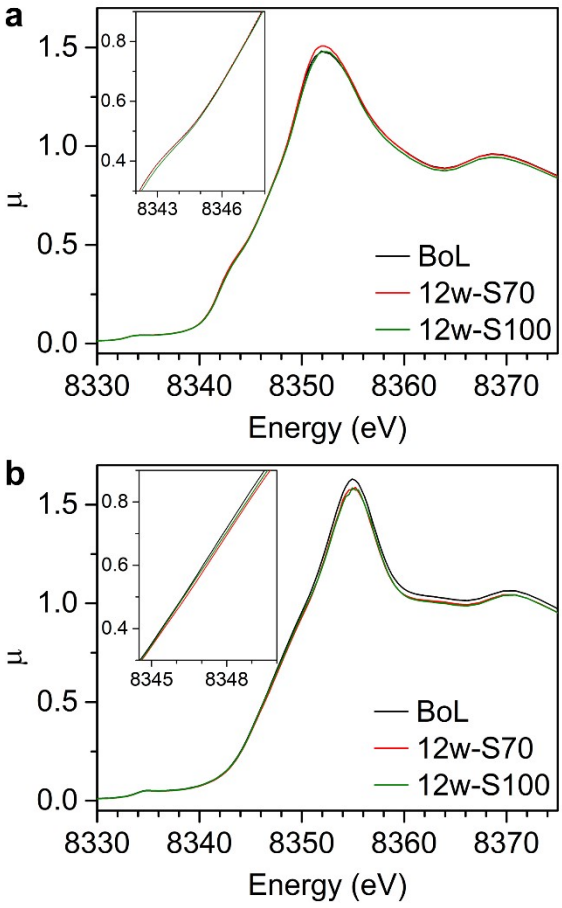

Fig. S7 Ex situ Ni K-edge XANES spectra of 12-week-stored NCM6 cathodes at the **a** discharge endpoint and **b** charge endpoint.

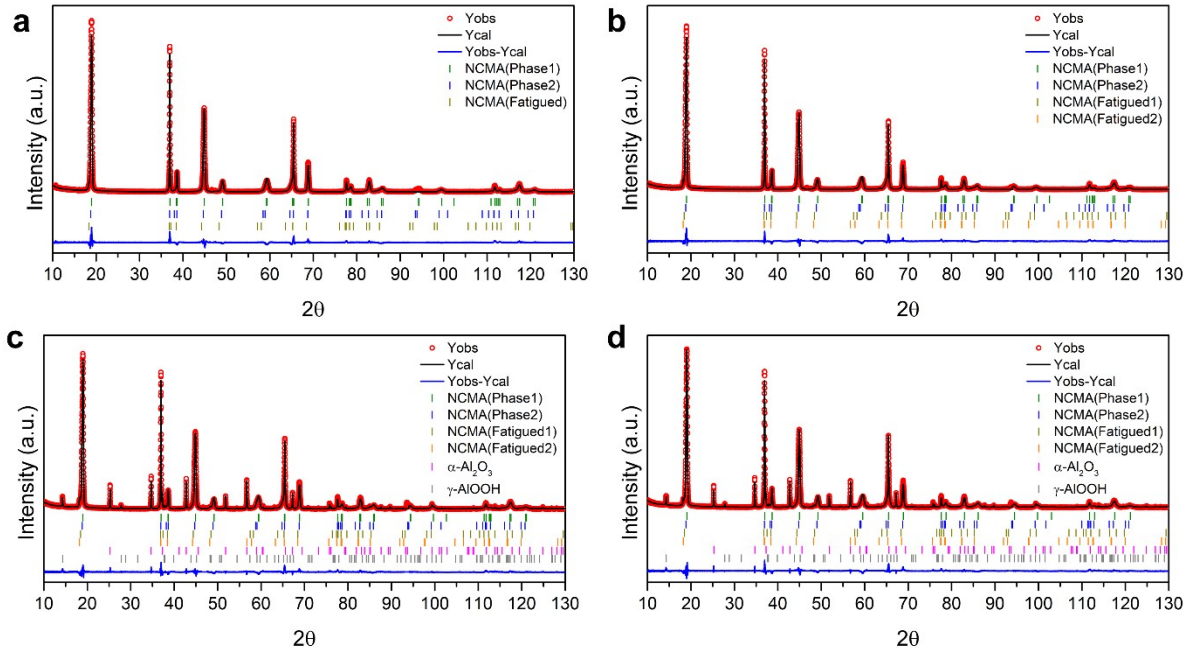

Fig. S8 Ex situ SXRD patterns and Rietveld refinement of **a** BoL, **b** 4w-S30, **c** 4w-S70, and **d** 4w-S100 NCMA8 cathodes at the charge endpoint. Two additional phases, α-Al_2O_3 and γ-AlOOH, were included for profile fitting, since the alumina-coated separator was used in the cells and coated ceramic was partially transferred onto the cathode surface.

Table S3 Rietveld refinement results of BoL NCMA8 cathode at the charge endpoint (Fig. S8a).

	Phase1	Phase2	Fatigued
a (Å)	2.81392(2)	2.81602(4)	2.8226(6)
c (Å)	13.8584(6)	14.031(2)	14.325(2)
V (Å^3)	95.032(4)	96.36(2)	98.84(3)
z_O	0.2642(1)	0.2660(3)	-
R_{Bragg}	5.37	4.70	10.5
Fraction(%)	78.7(1.6)	17.6(1.1)	3.6(2)
χ^2	4.07		

Table S4 Rietveld refinement results of 4w-S30 NCMA8 cathode at the charge endpoint (Fig. S8b).

	Phase1	Phase2	Fatigued1	Fatigued2
a (Å)	2.81374(2)	2.81575(3)	2.8222(5)	2.8194(5)
c (Å)	13.8373(7)	13.990(2)	14.273(1)	14.425(1)
V (Å^3)	94.874(5)	96.06(2)	98.32(3)	99.30(3)
z_O	0.2632(1)	0.2661(2)	-	-
R_{Bragg}	5.41	5.94	10.3	12.8
Fraction(%)	62.2(2.1)	32.2(1.7)	3.0(2)	2.7(2)
χ^2	4.01			

Table S5 Rietveld refinement results of 4w-S70 NCMA8 cathode at the charge endpoint (Fig. S8c).

	Phase1	Phase2	Fatigued1	Fatigued2
a (Å)	2.81395(2)	2.81602(3)	2.8218(6)	2.8205(5)
c (Å)	13.8227(8)	13.965(2)	14.243(2)	14.421(1)
V (Å^3)	94.789(6)	95.91(2)	98.21(3)	99.35(3)
z_O	0.2627(2)	0.2652(2)	-	-
R_{Bragg}	4.54	5.41	12.6	15.5
Fraction(%)	59.6(2.3)	33.5(2.1)	3.0(3)	3.9(2)
χ^2	4.47			

Table S6 Rietveld refinement results of 4w-S100 NCMA8 cathode at the charge endpoint (Fig. S8d).

	Phase1	Phase2	Fatigued1	Fatigued2
a (Å)	2.81441(2)	2.81683(3)	2.8275(9)	2.8188(7)
c (Å)	13.7865(8)	13.935(2)	14.198(3)	14.420(2)
V (Å^3)	94.571(5)	95.75(2)	98.30(5)	99.22(4)
z_O	0.2626(1)	0.2640(4)	-	-
R_{Bragg}	4.47	6.33	16.4	19.8
Fraction(%)	73.2(1.8)	20.3(1.4)	3.9(3)	2.6(2)
χ^2	4.99			

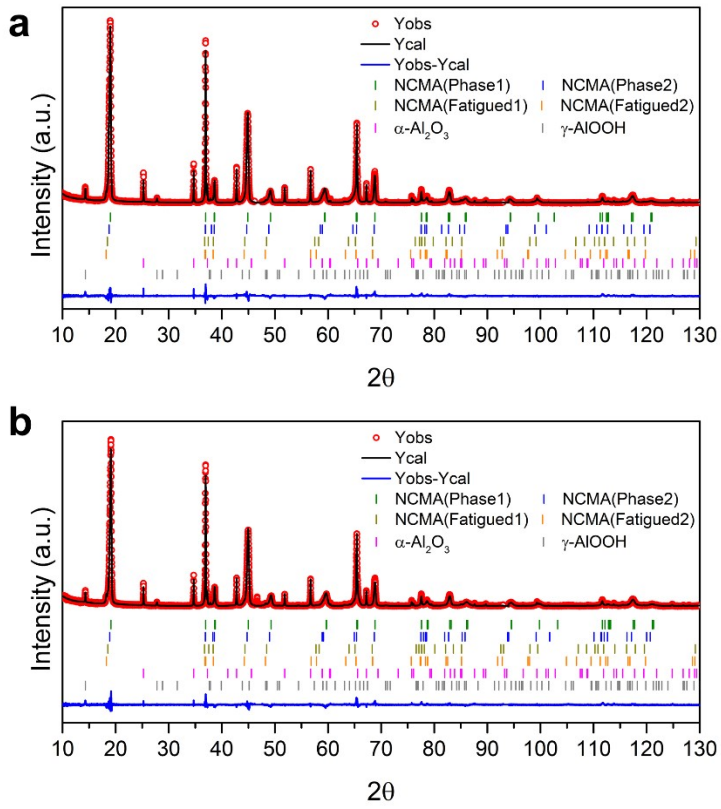

Fig. S9 Ex situ SXRD patterns and Rietveld refinement of 12-week-stored NCMA8 cathodes at the charge endpoint of **a** 12w-S70 and **b** 12w-S100. Two additional phases, α-Al_2O_3 and γ-AlOOH, were included for profile fitting, since the alumina-coated separator was used in the cells and coated ceramic was partially transferred onto the cathode surface.

Table S7 Rietveld refinement results of 12w-S70 NCMA8 cathode at the charge endpoint (Fig. S9a).

	Phase1	Phase2	Fatigued1	Fatigued2
a (Å)	2.81478(2)	2.81704(4)	2.8257(7)	2.8216(9)
c (Å)	13.8260(6)	14.002(2)	14.229(2)	14.417(2)
V ($Å^3$)	94.867(4)	96.23(1)	98.39(4)	99.40(5)
z_O	0.2627(2)	0.2647(3)	-	-
R_{Bragg}	4.81	6.39	15.8	21.6
Fraction(%)	67.0(1.2)	25.4(1.1)	4.7(5)	2.9(3)
χ^2	4.50			

Table S8 Rietveld refinement results of 12w-S100 NCMA8 cathode at the charge endpoint (Fig. S9b).

	Phase1	Phase2	Fatigued1	Fatigued2
a (Å)	2.81545(2)	2.81803(4)	2.8292(7)	2.8219(7)
c (Å)	13.7541(6)	13.924(2)	14.186(2)	14.394(2)
V ($Å^3$)	94.418(4)	95.76(1)	98.34(4)	99.26(4)
z_O	0.2637(2)	0.2640(3)	-	-
R_{Bragg}	5.05	6.06	8.93	12.7
Fraction(%)	65.6(1.4)	25.4(1.2)	5.7(5)	3.3(3)
χ^2	2.63			

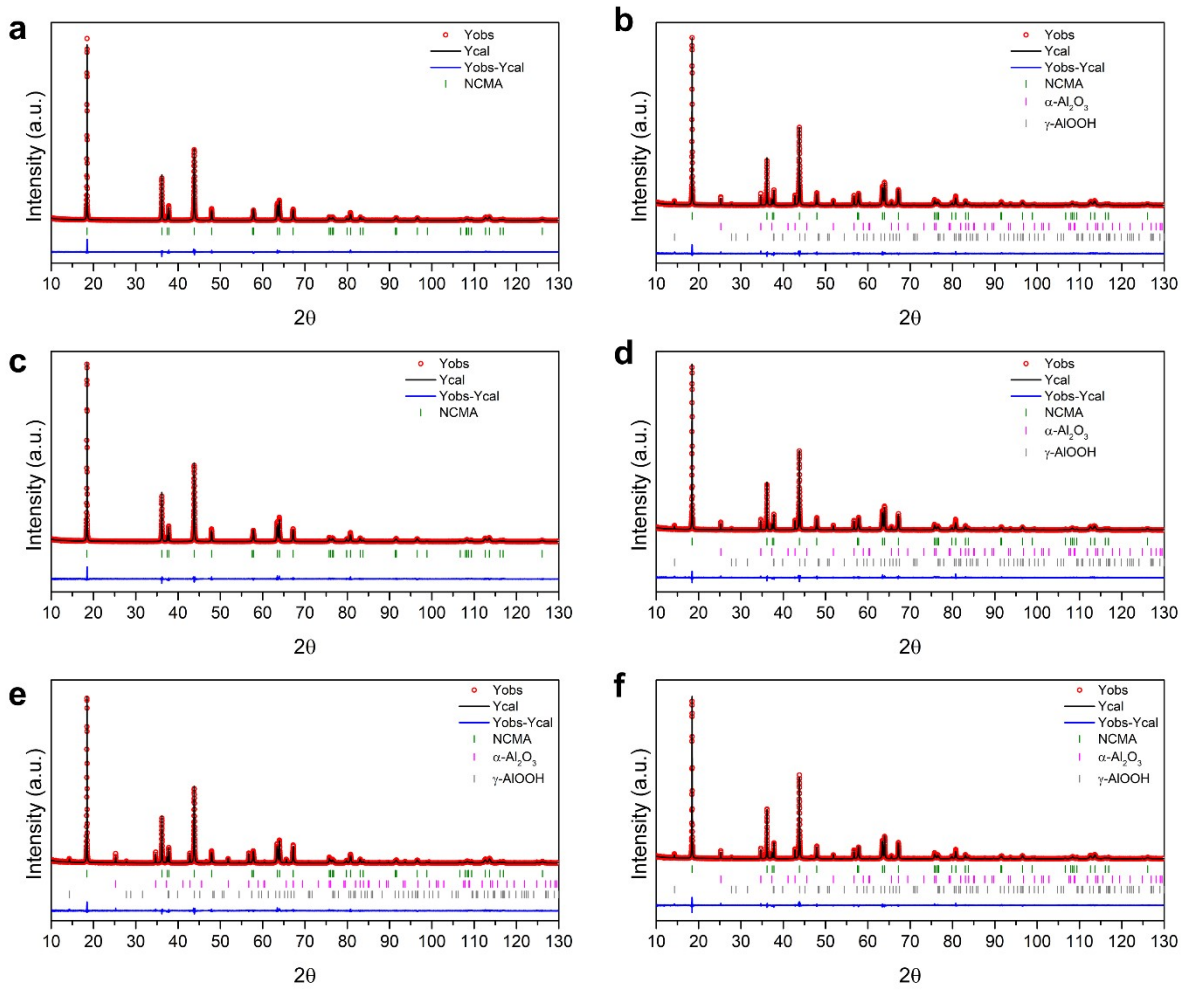

Fig. S10 Ex situ SXRD patterns of **a** BoL, **b** 4w-S30, **c** 4w-S70, **d** 4w-S100, **e** 12w-S70, and **f** 12w-S100 NCMA8 cathodes at the discharge endpoint. Two additional phases, α-Al_2O_3 and γ-AlOOH, were included for profile fitting, since the alumina-coated separator was used in the cells and coated ceramic was partially transferred onto the cathode surface.

Table S9 Rietveld refinement results of 4- and 12-week-stored NCMA8 cathodes at the discharge endpoint (Fig. S10).

	BoL	**4w-S30**	**4w-S70**	**4w-S100**	**12w-S70**	**12w-S100**
a (Å)	2.87406(1)	2.87347(1)	2.87328(1)	2.87334(1)	2.87216(1)	2.87258(1)
c (Å)	14.21942(9	14.22109(1	14.22314(1	14.22491(1	14.22846(1	14.23026(1
V (Å^3)	101.720(1)	101.690(1)	101.691(1)	101.708(1)	101.650(1)	101.692(1)
z_O	0.25915(7)	0.25869(8)	0.25916(8)	0.25890(9)	0.25924(8)	0.25859(8)
TM_{Li}	0.019(1)	0.025(1)	0.025(1)	0.030(1)	0.025(1)	0.027(1)
R_{Bragg}	3.53	2.49	3.55	3.65	3.35	3.01
χ^2	1.90	1.61	1.70	1.86	1.73	1.70

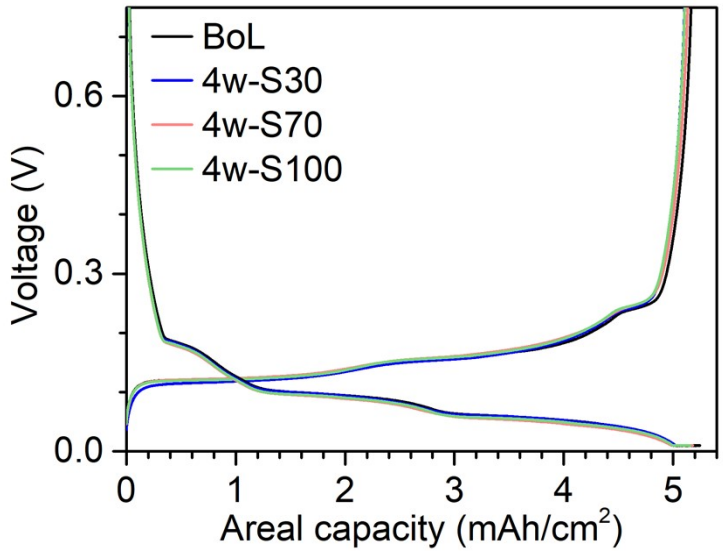

Fig. S11 Voltage profiles of graphite anodes retrieved from aged NCMA8/graphite cells at 0.5 mA cm^{-2} in the voltage range of 0.01–1.5V versus Li.

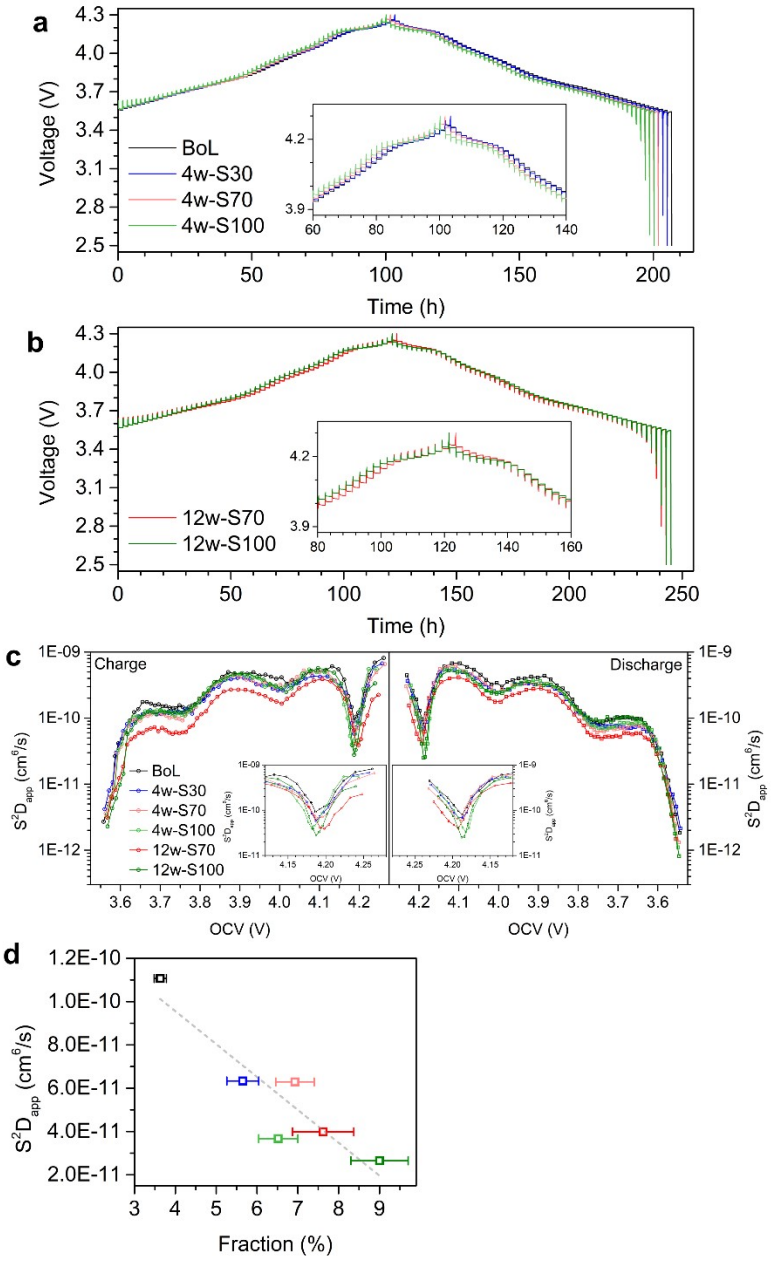

Fig. S12 GITT results of aged NCMA8 cathodes. **a**,**b** Voltage profiles during GITT measurements. **c** Calculated diffusion coefficients versus OCV measured during charging (left) and discharging (right). Since the accurate quantification of active surface area is not straightforward in thick porous electrodes, area-independent form of diffusivities (S^2D) are compared. Inset: expansion of diffusion coefficients at OCV ~4.2 V **d** Linear correlation between the local minima of the apparent diffusion coefficients at ~4.2 V and the fraction of fatigued phases obtained from ex situ SXRD at the charge endpoint.

Galvanostatic intermittent titration technique (GITT) was performed in a cathode half-cell after two CCCV charge-discharge cycles in the voltage range of 2.5–4.3 V at 0.1C, with the current calculated based on the capacity of BoL (~ 5 mAh cm^{-2}). For the GITT, a 0.1C current pulse was applied for 10 min followed by 90 min rest period in the voltage range of 2.5–4.3 V versus Li. For 12-week-stored cathode, 120 min of rest period was applied. Lithium diffusion coefficient was calculated at each pulse based on the following formula.[1,2]

$$D = \frac{4}{\pi}\left(\frac{iV_m}{FS}\right)^2\left[\frac{\left(dE_s/d\delta\right)}{\left(dE/d\sqrt{t}\right)}\right]^2 \qquad S^2D = \frac{4}{\pi}\left(\frac{iV_m}{F}\right)^2\left[\frac{\left(dE_s/d\delta\right)}{\left(dE/d\sqrt{t}\right)}\right]^2$$

Here, i is the pulse current (A), V_m is molar volume of active material ($cm^3\ mol^{-1}$), F is Faraday constant (96485 C mol^{-1}), and S is the active surface area for Li insertion (cm^2).

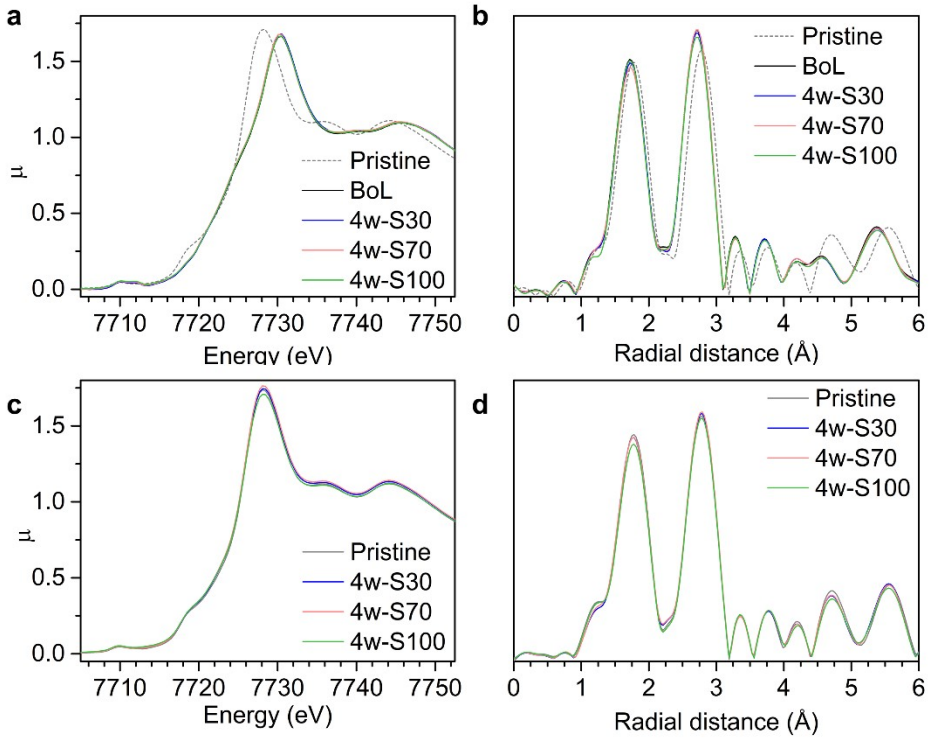

Fig. S13 Co K-edge XAFS results of 4-week-stored NCMA8 cathodes. **a** XANES spectra and **b** k^2-weighted FT-EXAFS magnitudes at the charge endpoint. **c** XANES spectra and **d** k^2-weighted FT-EXAFS magnitudes at the discharge endpoint. The Fourier transforms are corrected for the phase shifts of photoelectrons, to compare the radial distances with the actual distances estimated from XRD.

Table S10 Curve fitting results for Co K-edge EXAFS of 4-week-stored NCMA8 cathodes at the charge endpoint (Fig. S13b).

	Path	σ^2(Å^2)	R(Å)	χ_r^2	R-factor
BoL	Co-O	0.0027(5)	1.856(6)	91.2	0.0065
	Co-TM	0.0039(3)	2.793(6)		
4w-S30	Co-O	0.0030(6)	1.857(8)	62.2	0.0071
	Co-TM	0.0041(3)	2.791(8)		
4w-S70	Co-O	0.0031(5)	1.860(6)	45.3	0.0066
	Co-TM	0.0039(3)	2.795(7)		
4w-S100	Co-O	0.0027(5)	1.855(7)	68.1	0.0057
	Co-TM	0.0043(3)	2.789(8)		

Table S11 Curve fitting results for Co K-edge EXAFS of 4-week-stored NCMA8 cathodes at the discharge endpoint (Fig. S13d).

	Path	σ^2(Å^2)	R(Å)	χ_r^2	R-factor
Pristine	Co-O	0.0029(4)	1.902(4)	41.9	0.0035
	Co-TM	0.0046(2)	2.852(5)		
4w-S30	Co-O	0.0031(4)	1.899(4)	77.8	0.0031
	Co-TM	0.0045(2)	2.851(4)		
4w-S70	Co-O	0.0032(4)	1.899(5)	87.5	0.0037
	Co-TM	0.0044(2)	2.851(5)		
4w-S100	Co-O	0.0034(4)	1.901(5)	73.2	0.0038
	Co-TM	0.0046(3)	2.852(5)		

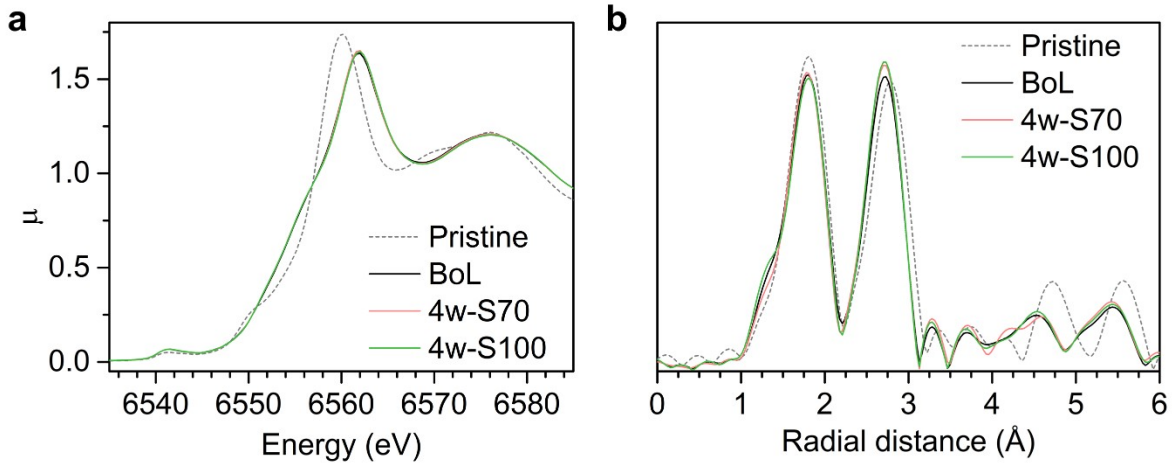

Fig. S14 Mn K-edge XAFS results of 4-week-stored NCMA8 cathodes. **a** XANES spectra and **b** k^2-weighted FT-EXAFS magnitudes at the charge endpoint. The Fourier transforms are corrected for the phase shifts of photoelectrons, to compare the radial distances with the actual distances estimated from XRD.

Table S12 Curve fitting results for Mn K-edge EXAFS of 4-week-stored NCMA8 cathodes at the charge endpoint (Fig. S14b).

	Path	σ^2 (Å^2)	R (Å)	χ_r^2	R-factor
Pristine	Mn-O	0.0041(7)	1.875(8)	145.9	0.0116
	Mn-TM	0.0063(5)	2.861(8)		
BoL	Mn-O	0.0046(7)	1.845(13)	56.6	0.0115
	Mn-TM	0.0068(5)	2.797(15)		
4w-S70	Mn-O	0.0046(6)	1.845(10)	34.5	0.0093
	Mn-TM	0.0065(4)	2.797(12)		
4w-S100	Mn-O	0.0050(7)	1.846(12)	43.9	0.0111
	Mn-TM	0.0066(5)	2.797(14)		

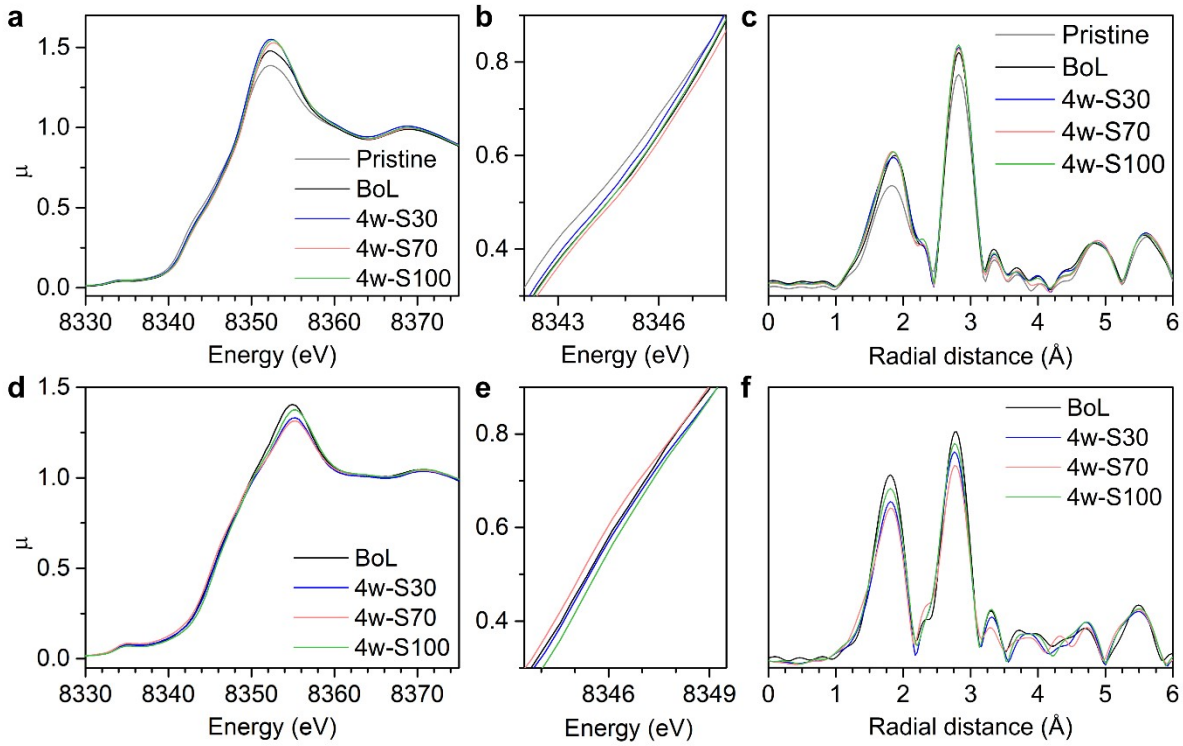

Fig. S15 Ni K-edge XAFS results of 4-week-stored NCMA8 cathodes. **a-c** Ni K-edge XAFS at the discharge endpoint. **a** Normalized Ni K-edge XANES spectra and **b** expansion of the edge region. **c** k^2-weighted FT-EXAFS magnitudes of Ni K-edge. **d-f** Ni K-edge XAFS at the charge endpoint. **d** Normalized Ni K-edge XANES spectra and **e** expansion of the edge region. **f** k^2-weighted FT-EXAFS magnitudes of Ni K-edge. The Fourier transforms are corrected for the phase shifts of photoelectrons, to compare the radial distances with the actual distances estimated from XRD.

Table S13 Curve fitting results for Ni K-edge EXAFS of 4-week-stored NCMA8 cathodes at the discharge endpoint (Fig. S15c).

	Path	σ^2 (Å^2)	R (Å)	χ_r^2	R-factor
Pristine	Ni-O	0.0129(13)	1.950(11)	38.4	0.0140
	Ni-TM	0.0058(3)	2.871(6)		
BoL	Ni-O	0.0101(8)	1.952(7)	7.2	0.0059
	Ni-TM	0.0057(2)	2.873(5)		
4w-S30	Ni-O	0.0106(8)	1.949(7)	40.3	0.0072
	Ni-TM	0.0056(2)	2.875(5)		
4w-S70	Ni-O	0.0097(7)	1.946(6)	29.0	0.0048
	Ni-TM	0.0054(2)	2.874(4)		
4w-S100	Ni-O	0.0099(7)	1.948(7)	56.5	0.0062
	Ni-TM	0.0054(2)	2.874(4)		

Table S14 Curve fitting results for Ni K-edge EXAFS of 4-week-stored NCMA8 cathodes at the charge endpoint (Fig. S15f).

	Path	σ^2 (Å^2)	R (Å)	χ_r^2	R-factor
BoL	Ni-O	0.0063(6)	1.866(8)	27.4	0.0033
	Ni-TM	0.0068(3)	2.810(9)		
4w-S30	Ni-O	0.0074(5)	1.864(7)	62.1	0.0031
	Ni-TM	0.0074(3)	2.802(7)		
4w-S70	Ni-O	0.0084(9)	1.871(10)	32.5	0.0099
	Ni-TM	0.0077(5)	2.822(10)		
4w-S100	Ni-O	0.0064(7)	1.859(9)	56.3	0.0043
	Ni-TM	0.0069(4)	2.797(10)		

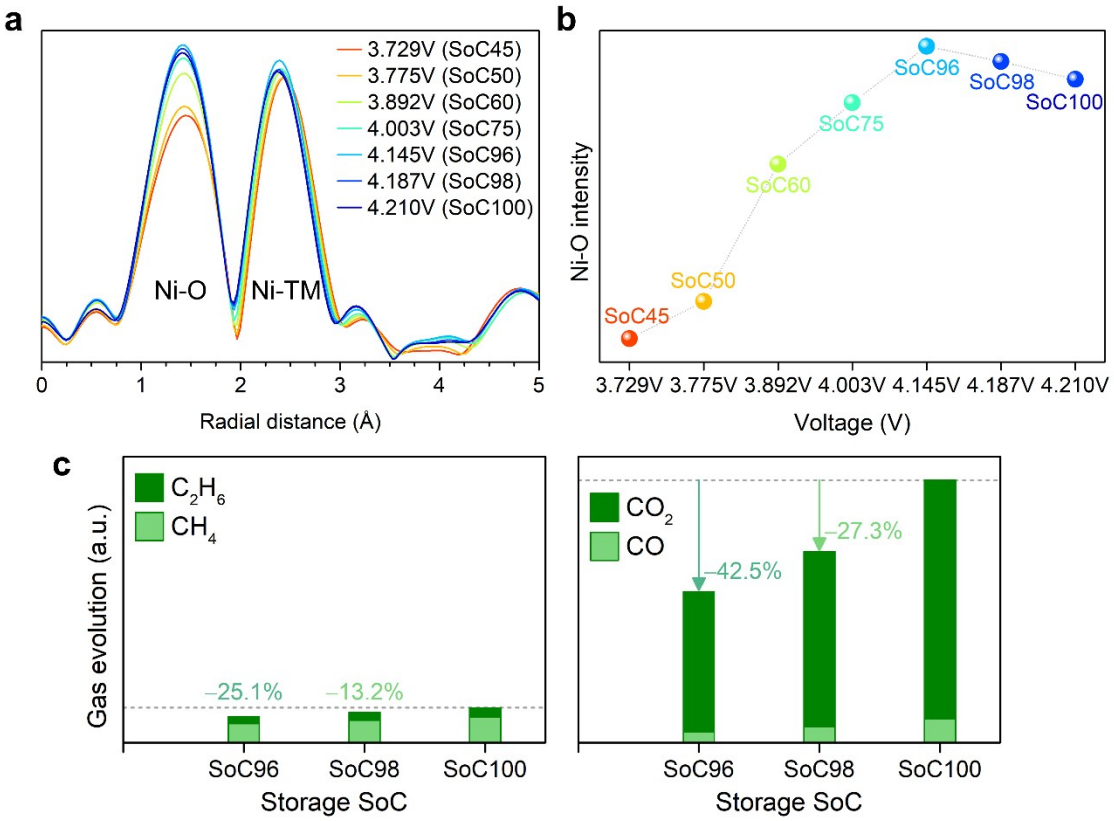

Fig. S16 a k^2-weighted FT-EXAFS magnitudes of Ni K-edge and **b** the intensity of Ni-O coordination shell as a function of the cell voltage and SoC. **c** Gas evolution in NCMA8/graphite cells during high SoC storage at 60 °C. The volume of alkanes (left), which mainly evolve from the anode, and CO/CO_2 (right), which mainly evolve from the cathode, are plotted with the same y-axis scales.

References

1 W. Weppner and R. A. Huggins, *J. Electrochem. Soc.*, 1977, **124**, 1569–1578.

2 S. Yang, X. Wang, X. Yang, Y. Bai, Z. Liu, H. Shu and Q. Wei, *Electrochim. Acta*, 2012, **66**, 88–93.